Design and optimization of a permanent magnet claw pole machine with concentrated winding and hybrid cores

Design and Optimization of a Permanent Magnet Claw Pole Machine with Concentrated Winding and Hybrid Cores

Chengcheng Liu[1*], Hongming Zhang[1], Dianli Lv[1*], Feng Niu[1], Gang Lei[2], Youhua Wang[1], Jianguo Zhu[2]

[1]State Key Laboratory for Reliability and Intelligence of Electrical Equipment Co built by Hebei University of Technology, Tianjin, 300131, China.(2016020@hebut.edu.cn, 13290408919@163.com, ldl79@hebut.edu.cn, niufeng@hebut.edu.cn, wangyi@hebut.edu.cn)

[2]School of Electrical Machinery and Electromechanical Integration, Sydney University of Science and Technology, Sydney, NSW 2000, Australia.(gang.lei@uts.edu.au, jianguo.zhu@sydney.edu.au)

***Abstract*—With the performance of soft magnetic composite (SMC) improves, there is a trend to develop permanent magnet claw pole machine (PMCPM) by using SMC cores in the past decades, as it is with complex 3D magnetic flux path. The traditional PMCPM (TPMCPM) needs to form the three phase operation by stacking three single phase modules in the axial direction and each of them need to be shifted with 120 degrees electrically to each other. In this paper, a PMCPM with concentrated winding (CWCPM) is proposed to overcome above constraints of the TPMCPM. Furthermore, the shielding layer is employed for reducing the flux leakage of CWCPM, and thus the performance of SL-CWCPM is improved. Considering these machines are with many design parameters, the multilevel sequential Taguchi method is employed and the sensitivity method with correction coefficient is employed for divide these design parameters into three groups. Lastly the hybrid silicon sheet and SMC cores is employed to increases the performance of CWCPM, and the concept of the hybrid material magnetic core for the PMCPM is verified by the experiment.**

***Index Terms*—Soft magnetic composite, permanent magnet claw pole machine, concentrated winding, sequential Taguchi method, hybrid material magnetic core.**

I. INTRODUCTION

By using the permanent magnet (PM) to produce the excitation magnetic field, the PM machine is with the advantages of high-power density, high efficiency and etc. and it is now employed for industrial, transportation, aerospace application and etc. According to the magnetic flux path diagram, the PM machine can have radial flux, axial flux and transverse flux [1]-[3]. By using the global ring winding, and 3D magnetic flux structure, the torque coefficient of PM machine with transverse flux is very high. However, it is difficult to manufacture the transverse flux machine by using the traditional silicon sheets [4]. Recently, with the performance improvement of soft magnetic composite (SMC), the transverse flux machine can be easily made by using the SMC [5]-[7].

SMC is a relatively new soft magnetic material, it is with magnetic isotropy and low eddy current loss characteristic. By using the powder metallurgy technology, the production cost of electrical machine with SMC cores will be reduced greatly[8]. However, the SMC is with the low permeability, high hysteresis loss characteristic as well. In the past decades, many works were done on developing high performance electrical machines with SMC cores[9]. Compared with other electrical machines, the transverse flux permanent magnet machine can fully follow the design guidelines of electrical machine with SMC cores, e.g. the 3D magnetic flux, high operation frequency, and PM excitation. Using SMC exclusively for the stator core of the claw-pole motor will have the problems of high failure rate of stator core compression molding and high cost of mold making. Therefore, literature [10] proposes the basic structure of hybrid material core motors, focusing in with comparing the electromagnetic performance of hybrid material core claw-pole motors with full SMC claw-pole motors.

Permanent magnet claw pole machine (PMCPM) is a special kind of transverse flux machine, which is with better performance[11]. In the past decades, many scholars have improved the structure of PMCPM to enhance the electromagnetic performance of the motor. Literature [12] proposes using methods such as cutting and bonding silicon steel sheets to fabricate stator claw poles for claw pole motors, but there are problems such as perpendicular magnetic density of the splicing surface. Literature [13] compared the effect of four different rotor permanent magnet arrangement methods on the electromagnetic performance of the motor, and the results showed that the surface-mounted structure has a higher average torque. Literature [14] proposed a new type of transverse flux flux-switching claw-pole motor by placing permanent magnets in the stator core, which increases the rotor mechanical strength, but the torque of this type of motor is lower under the same amount of permanent magnets. According to the main magnetic air gap flux direction, the PMCPM includes the traditional radial flux and axial air flux PMCPM[15]. Both of these two machines are designed with the global ring winding and for forming three phase symmetrical operation three single phase modules of the PMCPM are generally required to be arranged in the axial direction[16].

To reduce the cogging torque and torque ripple of the PMCPM, the unequal stator claw pole teeth and PM skew structure are generally utilized. Considering the performance calculation of PMCPM by using 3D FEM is time consuming and the PMCPM is with many design parameters, the multilevel design optimization method is employed for the design

optimization of PMCPM. To overcome the design parameters uncertain of the PMCPM, the robust design optimization method is used to reduce the manufacturing errors[17]. To improve the torque ability of PMCPM furthermore, the S shape winding is proposed to add the cross-sectional area of the slot and thus the machine is a much higher compact design[18].

The most researches for the PMCPM are focused on studying the stator and PM structure, while seldom for the winding design and optimization. For the traditional PMCPM, the global rind winding is employed, and their three phase modules are arranged in the axial direction but from the magnetic circuit viewpoint they are independent. For improving the performance of PMCPM, it needs to be designed with long axial length. Moreover, it is high torque ripple as its special structure.

In this paper, a special PMCPM with concentrated winding (CWCPM) is proposed, where the three symmetrical phase operation is formed in the circumferential way, therefore the PMCPM has the potential to be designed with short axial length to achieve better torque performance. Furthermore, the shielding layer is used to reduce the flux leakage in the CWCPM, and the hybrid silicon sheet-SMC cores is proposed to improve the torque ability of CWCPM. Finally the performance analysis method of Traditional claw pole motor (TCPM) with hybrid silicon sheet and SMC cores is verified by the experiment.

II. Main Magnetic Structure of CWCPM

A. Structure design

Fig.1 shows the main structure of TCPM. As shown, the machine consists of three identical single-phase modules arranged in coaxial rows, and the rows of the three single-phase motors are spatially separated from each other by an electrical angle of 120deg.The material of the motor is a soft magnetic composite, specifically on stator as shown in Fig. 1(b) is formed by using two stator claw poles and one global winding is installed in between these two stator claw poles. The rotor is made by using the silicon sheets, and the NdfeB PMs are mounted on the surface of the rotor.

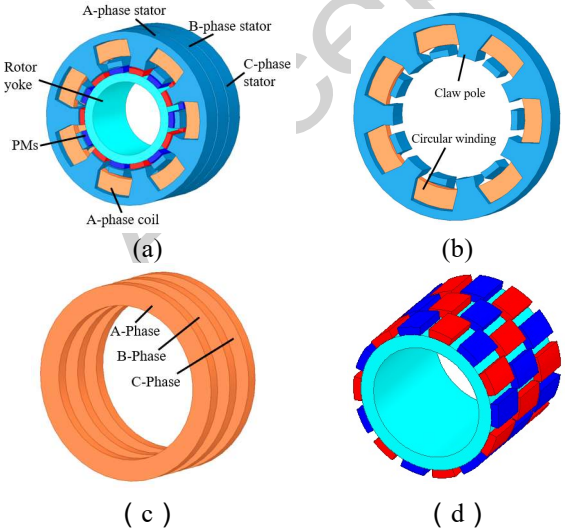

Fig.1. Main structure of TCPM. (a) three phase structure (b) single module (c) three phase coil (d) rotor structure.

Fig. 2 shows the structure of the proposed CWCPM. As shown, the machine composes of stator core, concentrated winding, PM rotor core. Fig. 2(b) shows the one phase module of CWCPM, it can be seen that one phase module of this CWCPM is composed of three groups of stator claw poles and one phase concentrated winding as shown in Fig. 2(c). The difference between the proposed CWCPM and TCPM is the way to form the three phases symmetrical operation. For the CWCPM, its adjacent stators are shifted with 120° (electrical) from each other. Similar to the TCPM, the rotor of CWCPM is made by using the silicon sheets, and the NdfeB are mounted on the surface of the rotor. It can be seen that there is 14 PMs are required for the CWCPM, and there are 9 claw poles for the stator side, therefore there are 5 PMs can't form closed flux circuit, and the flux leakage is serious for this kind of machine.

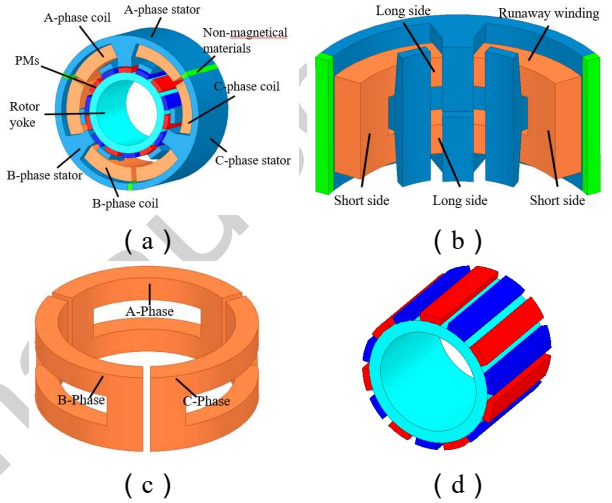

Fig.2. Main structure of CWCPM (a) three phase structure (b) single module (c) three phase coil (d) rotor structure.

To reduce the flux leakage of CWCPM, three blocks are made and installed in between the rotor PM and stators. Compared with the initial design, there are only 2 PMs can't form closed flux circuit, as shown in Fig.3 In order to compare the performance of TCPM, CWCPM and SL-CWCPM, the stator outer diameter, axial length and amount of employed PMs of these machines are the same. Table I shows the main structural parameters of TCPM and CWCPM.

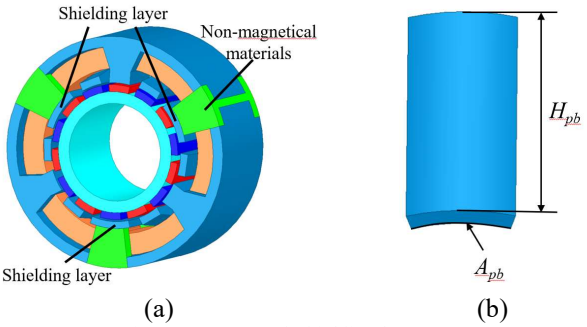

Fig.3. Structure of SL-CWCPM and Shielding layer

TABLE I
STRUCTURE PARAMETERS

Symbol	Describe	Unit	TCPM	CWCPM
R_{so}	Stator Outer diameter	mm	50	50
R_{si}	Stator inner diameter	mm	30	30
L_{gap}	Air gap length	mm	0.85	0.85

H_{pm}	PM radial length	mm	3	3
A_{pm}	PM circumferential width	deg	8.5	8.5
L_{PM}	PM axial length	mm	15	48
L_{ry}	Rotor yoke thickness	mm	9	9
L_{tall}	Shaft length	mm	15	48

B. Magnetic flux path and equivalent magnetic circuit

As shown, TCPM and CWCPM have different stator structures and thus different flux paths and equivalent magnetic circuit. For TCPM, its three phase modules are independent from each other, therefore for the simplification only one phase module is required for the performance analyzing. Fig. 4 shows the main magnetic flux path of TCPM, and CWCPM.

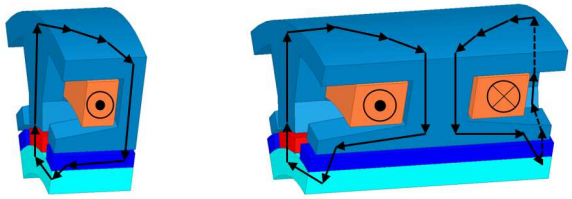

(a) TCPM (b) CWCPM

Fig.4. Main flux path under single-phase single pole

According to the magnetic flux path shown in Fig.4(b), the equivalent magnetic circuit model of CWCPM can be built as shown in Fig.5, where R_r, R_s, R/min denote the stator, rotor and PM equivalent reluctance respectively, R_g, R_{ct}, R_{ce} denote the air gap, stator tooth top, stator tooth yoke equivalent reluctance respectively, $R_{\sigma 1}$, $R_{\sigma 2}$, $R_{\sigma 3}$ denote the PM and rotor silicon steel direct equivalent leakage reluctance, the PM inter-pole equivalent leakage reluctance and the stator claw inter-pole equivalent leakage reluctance respectively, F_m, F_a represent the PM magnet potential and armature magnet potential respectively.

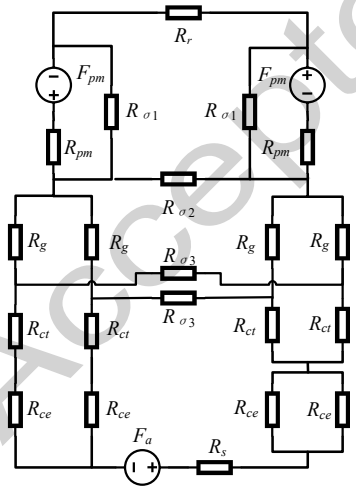

Fig.5. Equivalent magnetic circuit of CWCPM

C. Operation principle analysis

Fig.6 shows the operation process of CWCPM. The main magnetic circuit of the new inner rotor radial flux claw pole motor includes two magnetic flux paths, each of which is the same as the traditional inner rotor radial flux claw pole motor. The magnetic flux starts from the N-pole permanent magnet of the rotor, passes through the air gap, and enters the stator claw pole teeth of the two head to head stator claw poles. The two parts of the magnetic flux enter the stator claw pole wall through the root of the stator claw pole, and enters the stator yoke through the stator claw pole wall, The magnetic flux converges in two parts of the adjacent back-to-back stator claw pole walls. After the magnetic flux flows to the root of the back-to-back stator claw pole, it enters the teeth of the two stator claw poles respectively. The two parts of the magnetic flux enter the rotor S-pole permanent magnet through the fixed air gap, and return to the rotor N-pole permanent magnet through the rotor yoke, forming a closed circuit. The magnetic path direction of the main magnetic flux undergoes six changes, passing through two air gaps, four stator pawl poles, two permanent magnets, stator yoke, and rotor yoke.

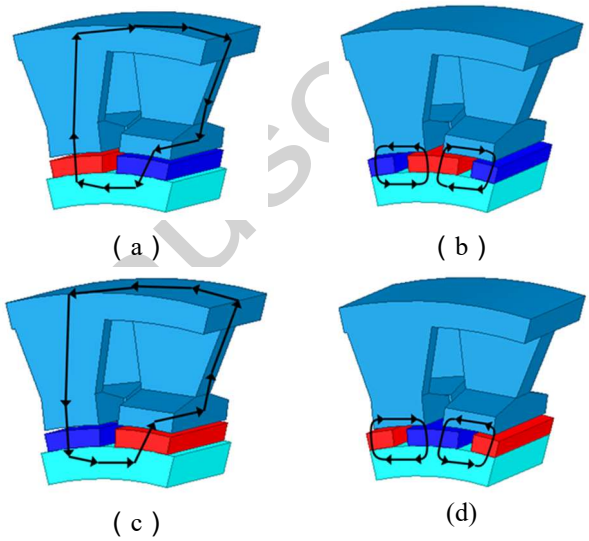

(a) (b) (c) (d)

Fig.6. Main flux path of CWCPM. (a) PM flux (positive maximum). (b) PM flux (zero). (c) PM flux (negative maximum). (d) PM flux (zero).

D. Simplified power equation analysis

In the PM machine, the main electromagnetic relationships can be expressed by the following equations. In this paper, the optimum brushless dc model is used, in which the phase current is controlled to have the same phase angle as the phase back electromotive force (EMF). The electromagnetic power of the PM machine can be expressed as

$$\begin{aligned} P_{em} &= \frac{m}{T}\int_0^T e(t)i(t)dt \\ &= \frac{m}{T}\int_0^T E_m I_m \sin(\frac{2\pi}{T}t)\sin(\frac{2\pi}{T}t)dt \\ &= \frac{m}{2}E_m I_m \end{aligned} \tag{1}$$

where, m is the number of phases, T the electric period, E_m the the magnitude of EMF, and I_m the phase current amplitude.

The back EMF of the PM motor is proportional to the variation of the magnetic flux linkage with time, and the magnetic flux linkage can be expressed as

$$\psi = N_{coil}\varphi_m \cos(\frac{2\pi}{T}t) \tag{2}$$

where φ_m is the magnitude of the PMflux linkage and N_{coil} the number of turns per phase winding.

The back EMF can be expressed as:

$$E = -\frac{d\psi}{dt} = \frac{2\pi N_{coil}\varphi_m}{T}\sin(\frac{2\pi}{T}t) \tag{3}$$

The phase current can be expressed as:

$$I = I_m \sin(\frac{2\pi}{T}t) = J_c A_{coil} k_{sf} \sin(\frac{2\pi}{T}t) \tag{4}$$

where, I_m is phase current amplitude, J_c the phase current density, A_{coil} the phase winding cross-sectional area, and k_{sf} the slot filling rate.

According to equations (1) - (4), the electromagnetic power and electromagnetic torque of the PM motor can be deduced further as:

$$P_e = \frac{m}{2} N_{coil} P_r \omega_r \varphi_m J_c A_{coil} k_{sf} \tag{5}$$

$$T_e = \frac{P_e}{w_r} = \frac{m}{2} N_{coil} P_r \varphi_m J_c A_{coil} k_{sf} \tag{6}$$

where P_r is the pole pair number. As shown the torque of PM machine is determined by its PM flux linkage, winding cross sectional area and the applied current density. Claw pole machine is a special kind of transverse flux machine, its PM flux linkage is determined by the PM flux, specifically it can be calculated by,

$$\psi_{pm} = 2P_r N_{coil} R_s \int_{-\frac{Ls}{2}}^{\frac{Ls}{2}} \int_{\theta_i - \frac{\theta_0}{2}}^{\theta_{i+1} - \frac{\theta_0}{2}} Br(r,\theta) d\theta dL_s \tag{7}$$

where p is the number of pole pairs, N the number of windings per slot, L_{sy} the axial length of the claw pole motor, R_s the stator inner diameter, θ_0 the angle between the adjacent stator claw pole sides, and θ_i the angle between the center of the ith claw pole and the central axis of the winding.

For the simplification, the flux leakage and uneven air gap magnetic flux distribution along its axial direction are ignored, and the above equation can be simplified as,

$$\psi_{pm} = 2P_r N_{coil} R_s B_r S_{ct} \tag{8}$$

where B_r is the magnetic flux density vertical to the stator claw pole teeth, and S_{ct} the surface area of the stator claw pole teeth. The area of stator claw pole teeth and winding sectional can be determined by the main dimensions of the electrical machine, Fig.7 shows the main dimensions of the TCPM and CWCPM. Table II tabulates the main dimensions.

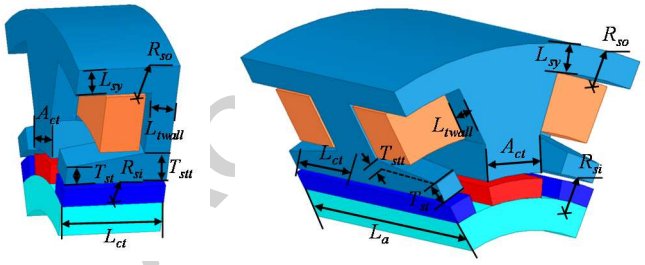

(a) (b)

Fig.7. Main dimensional parameters of TCPM and CWCPM. (a)TCPM (b) CWCPM

TABLE II
DIMENSIONAL PARAMETERS AND COEFFICIENTS

Parameter	Units	TCPM	CWCPM
L_a	mm	48	48
L_{twall}	mm	4	6
R_{so}	mm	50	50
R_{si}	mm	30	30
L_{sy}	mm	4	4
T_{st}	mm	2.5	2.5
T_{stt}	mm	1.5	1.5
L_{ct}	mm	16	24
A_{ct}	mm	5.8	5.8
α_p	--	0.85	0.85
k_{coil}	--	0.96	0.96
k_l	--	1	1
P_r	--	7	--
P_c	--	--	6

Based on the equations (1)-(8) and the main design parameters, the electromagnetic torque of TCPM can be deduced as,

$$T_{TCPM} = K_{TCPM} L_{ct1} R_{si} (L_{ct1} - 2L_{twall1}) \times (R_{so} - R_{si} - L_{sy} - T_{st} - T_{stt}) \tag{9}$$

$$K_{TCPM} = \frac{1}{2}\pi m P_r \alpha_p k_{coil} k_l k_{sf} J_c B_r \tag{10}$$

Where, L_a is the axial length of the machine, L_{twall} the thickness of stator claw pole wall, L_{ct} the axial length of the stator claw pole teeth, R_{so} the stator outer radius, Rsi the stator inner radius, L_{sy} the stator yoke thickness, T_{st} the thickness of top part of stator claw pole teeth, T_{stt} the thickness of end part of stator claw pole teeth, A_{ct} the width of stator claw pole teeth, α_p the pole arc coefficient, k_{coil} the winding factor, k the leakage coefficient, aand B_g the magnitude of air gap flux density.

Based on the design experience of claw pole machine, the maximum torque ability will be achieved when the axial length stator claw pole wall equals the half of the slot width, then the axial length of the stator claw pole wall can be determined as,

$$L_{ct1} = \frac{L_a}{m} \tag{11}$$

$$L_{twall1} = \frac{L_{ct}}{4} = \frac{1}{12} L_a \tag{12}$$

The electromagnetic torque of CWCPM can be calculated by：

$$T_{CWCPM} = K_{cpm} L_{ct2} R_{si} (L_{ct2} - 2L_{twall2}) \times (R_{so} - R_{si} - L_{sy} - T_{st} - T_{stt}) \tag{13}$$

$$K_{CWCPM} = \frac{103}{360}\pi m P_r \alpha_p k_{coil} k_l k_{sf} J_c B_r \tag{14}$$

Its stator claw pole wall thickness and its axial length of stator claw pole teeth can be determined by,

$$L_{ct2} = \frac{L_a}{2} \tag{15}$$

$$L_{twall2} = \frac{L_{ct}}{4} = \frac{L_a}{8} \tag{16}$$

According to equations (9) - (16) , it can be seen that the torque of TCPM and CWCPM are influenced by their main design parameters. Kept the stator outer radius, stator inner radials, stator yoke thickness and some other key dimensions affect the strength of the SMC claw pole the same, the torque relationship of these two machines can be expressed by,

$$\frac{T_{TCPM}}{T_{RWCPM}} = \frac{180L_{ct1}(L_a/m - 2L_{twall1})}{103L_{ct2}(L_a/2 - 2L_{twall2})} < 1 \quad (17)$$

As shown in equation (17), when keeping the main design parameters of these two machine the same, and let the thickness of stator claw pole equals about the half of the slot width, the calculated torque of TCPM is about 0.776 times of that of CWCPM. Therefore, the proposed machine is with better performance.

III. Design Optimization and Performance Analysis of CWCPM

A. Design Optimization

As the main magnetic structure of TCPM, and CWCPM are very complex, 3D finite element method is an effective way to obtain their main magnetic performance. However, compared with traditional PM machine, these two machines are with more design parameters and many of them are coupled with each other, therefore in the design optimization of TCPM and CWCPM, it is very difficult to obtain the optimal design by using the traditional sequential optimization method. On the other hand, it is time consuming to using the global optimization method for optimizing the 3D flux machines. In this paper, multilevel sequential Taguchi method is employed for the design optimization of TCPM and CWCPM, its flow chart is shown in Fig.8.

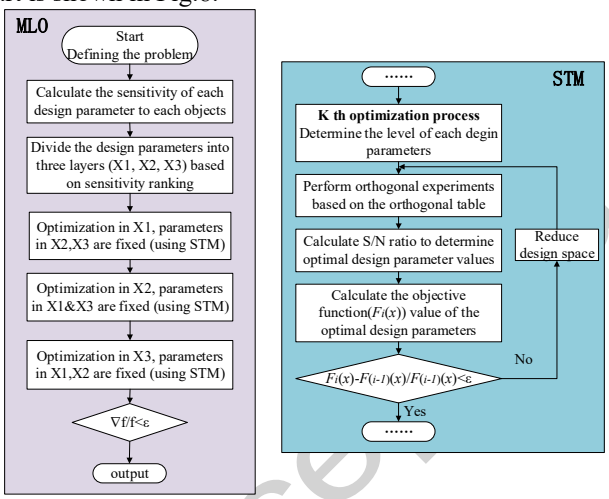

Fig.8. Multilevel sequential Taguchi optimization flow chart.

The objectives and constraints of the optimization process are shown as,

$$\min \quad F(x) = w_1 \frac{T_{ave\_ini}}{T_{ave}} + w_2 \frac{T_{cogging}}{T_{cogging\_ini}} + w_3 \frac{\eta_{ini}}{\eta} \quad (18)$$

$$s.t. \quad g_1(x) = 0.8 - \cos\varphi < 0$$

where T_{ave_ini}, $T_{cogging\_ini}$, η_{ini} are the initial values of average torque, cogging torque and efficiency respectively, T_{ave}, $T_{cogging}$, η are the average torque, cogging torque and efficiency at the design point respectively, cosφ is the power factor at the design point, w_1, w_2 and w_3 are the weighting coefficients, selected in this paper as 0.4, 0.4 and 0.2 respectively.

The key of multilevel design optimization is to divide the design parameters into different groups, and the sensitivity analysis method is commonly employed. The traditional sensitivity analysis method includes local sensitivity analysis and global sensitivity analysis method. In this paper, the local sensitivity analysis method is employed to calculate the sensitivity of the design parameters to the objective function, assuming that the objective to be optimized is F(x), such as average torque, cogging torque or efficiency. Where x=[x_1, x_2, x_3,..., x_n] denotes the design parameters of the motor, where n is the design parameter dimension. Then the local sensitivity of S_i at x_{i0} for the i-th parameter x_i can be expressed as

$$S_i = \partial F(x)/\partial x_i\big|_{x=x_0} \quad (19)$$

The greater S_i the greater the sensitivity of parameter xi to the target F(x), and then x_i should be considered as a key consideration in the optimal design [19]. By using 3D finite element method, the performance of CWCPM with the determined design parameters can be obtained, and equation (19) can be rewritten as

$$S_i = \frac{F(x_{i0} \pm \Delta x_i) - F(x_{i0})}{\pm \Delta x_i} \quad (20)$$

where Δx_i is the increment of design parameter of x_i.

Considering that different parameters have different units, in order to make the calculated sensitivity of different design parameters comparable, equations (19) and (20) can be written in a normalized form as follows:

$$S_i = \frac{\partial F(x)/F(x)}{\partial x_i / x_i} \quad (21)$$

$$S_i = \frac{(F(x_{i0} \pm \Delta x_i) - F(x_{i0}))/F(x_{i0})}{(\pm \Delta x_i)/x_i} = \frac{\Delta F(x_i)}{\delta F(x_{i0})} \quad (22)$$

where, δ is the range of variation of x_i. In this paper, it is ±1/10%.

The sensitivity of the design parameters calculated using Eqs. (21)-(22) is strongly influenced by the characteristics of the objective itself, such as for cogging torque and average torque, which may vary by 10%-20% at different design points, while for efficiency, the variation is usually around 1%. Therefore, evaluating the sensitivity by equation (22) will make the sensitivity of the parameters for cogging torque and average torque very large while the sensitivity of the design parameters for efficiency too small. Though, the calculated sensitivity for single objective is accurate, the sensitivity of the design parameters to efficiency cannot be fully considered when evaluating the combined sensitivity of multiple objectives. In this paper the correction coefficients of different objectives is employed to evaluate the combined sensitivity. For the kth objective F_k (x), its sensitivity correction coefficient can be expressed as

$$w_k = \frac{F_k(x_i)}{F_{kU}(x) - F_{kL}(x)} \quad (23)$$

where $F_{kU}(x)$ and $F_{kL}(x)$ are the maximum and minimum values of the objective function of F_x (x_i) for all design points, F_k (x_i) is the value of the objective function at the initial design point.

Combining Eqs. (21)-(23), the formula for sensitivity analysis with correction factors can be obtained as

$$S_{ik} = w_k S_i = \frac{F_k(x_i)\Delta F(x_i)}{\delta(F_{kU}(x) - F_{kL}(x))F(x_{i0})} \quad (24)$$

where S_{ik} denotes the sensitivity of parameter x_i to the object $F_k(x_i)$.

The combined sensitivity of parameter x_i to multiple objectives can be expressed as

$$MOS_i = \sum_{k=1}^{N} S_{ik} \tag{25}$$

Taking CWCPM as an example, Fig. 9 shows its eight main design parameters. In this paper, the average torque, cogging torque and efficiency are determined for optimization. The sensitivity of the design parameters to the average torque ($S(T_{ave})$), the sensitivity of the design parameters to the cogging torque ($S(T_{cogging})$) and the sensitivity of the design parameters to the efficiency ($S(\eta)$) are calculated respectively, and the combined sensitivity of multiple objectives (MOS) is calculated

TABLE III
CALCULATED RESULTS OF CONVENTIONAL SENSITIVITY ANALYSIS

	$S(T_{ave})$	$S(T_{cogging})$	$S(\eta)$	MOS
A_1	0.0792	0.232	0.0102	0.3218
W_{tall}	0.612	0.488	0.0225	1.12
L_{ry}	0.680	0.466	0.0561	1.20
L_{twall}	1.516	1.42	0.0532	2.99
R_{si}	1.807	4.85	0.0473	6.70
T_{st}	0.544	0.220	0.0398	0.803
T_{stt}	0.875	0.256	0.0700	1.20
A_{pm}	0.836	2.74	0.0646	3.65

Table IV
CALCULATED RESULTS OF SENSITIVITY ANALYSIS WITH CORRECTION FACTORS

	$S(T_{ave})$	$S(T_{cogging})$	$S(\eta)$	MOS
A_1	0.0965	0.119	0.406	0.621
W_{tall}	0.745	0.250	0.887	1.88
L_{ry}	0.828	0.239	2.22	3.29
L_{twall}	1.85	0.726	2.10	4.67
R_{si}	2.20	2.49	1.86	6.55
T_{st}	0.662	0.113	1.57	2.34
T_{stt}	1.07	0.131	2.76	3.96
A_{pm}	1.02	1.41	2.55	4.98

Table III and Table IV show calculated sensitivity analysis results by using the conventional sensitivity method and improved method with taking the correction factors into consideration. It can be seen that, for the sensitivity analysis of single objective both these two methods output same results, however for the combined sensitivity analysis the ranking results by using the improved method is more reasonable. According to the calculated sensitivity results shown in Table IV, the design parameters of CWCPM are divided into three groups, specifically the Rsi, Ltwall, Apm with high sensitivity are determined for X1 group, the Tstt, Lry and Tst with middle sensitivity are selected for X2 group, and the Wtall and A1 with low sensitivity are selected for X3 group. By using the proposed sensitivity method and sequential Taguchi method, both CWCPM and TCPM are optimized, and based on the optimized CWCPM, the shielding layer of SL-CWCPM is optimized as well. Table V shows the main design parameters of these optimized machines.

Table V
OPTIMAL PARAMETERS OF THE THREE MOTORS

Parameters	Unit	TCPM	CWCPM	SL-CWCPM
R_{si}	mm	30	30	30
W_{tall}	mm	9.5	9.61	9.61
L_{ry}	mm	5	5	5
L_{twall}	mm	3.75	6	6
A_1	deg	24	22	22
T_{st}	mm	2	2.4	2.4
T_{stt}	mm	3	3	3
A_{pm}	deg	18.5	18.4	18.4
A_{SL}	deg	-	-	7
H_{SL}	mm	-	-	2.4

B. Performance Comparison

Fig.9(a)-(b) compares the no-load PM flux linkage and no-load back EMF of these motors. As shown, TCPM is with the highest PM flux linkage, because to obtain three phase symmetrical operation the stator of CWCPM is shifted in the circumferential way, then some of PMs are not utilized to produce the PM flux linkages. In addition, by adding the shielding layer the flux leakage in CWCPM is reduced, therefore the PM flux linkage of SL-CWCPM is higher than that of CWCPM. However, due to the higher slot area, the torque ability of CWCPM is better than that of TCPM though its PM flux linkage is lower as shown in Fig.9(c). As shown, the average torque of CWCPM is 2.85 N·m, and that of TCPM is about 2.58 N·m which is a 10.5% improvement in torque performance, when the current density equals 6 A/mm2. In addition, by adding the shield layer, the torque of SL-CWCPM is further improved, and the torque of SL-CWCPM is 3.10N·m at rated operating conditions, which is 20.2% higher compared to TCPM.

Fig. 9(d) shows the power factor of these motors. It can be seen that the CWCPM has a lower power factor compared to the TCPM, because the CWCPM has fewer stator claw poles, resulting in a larger leakage flux and leakage inductance. The addition of the shield layer reduces the leakage flux but making the reluctance of main magnetic circuit smaller, therefore compared with CWCPM the power factor of SL-CWCPM increases. The calculated inductance of TCPM, CWCPM and SL-CWCPM are 323 nH, 365 nH and 389 nH respectively. Fig.9(e) and (f) shows the cogging torque and torque waveforms when the applied current density equals 6 A/mm2 of these motors. As shown, the magnitude of the cogging torque of the CWCPM is 0.19 N·m, which is 56.8% lower compared to 0.44 N·m of the TCPM, while cogging torque of the SL-CWCPM is 0.35N·m, which is 20.5% lower compared to the TCPM. It can be seen that the CWCPM is with lower cogging torque and torque ripple, the main reason is that the slotting factor is not high for the CWCPM as it is less stator claw poles.

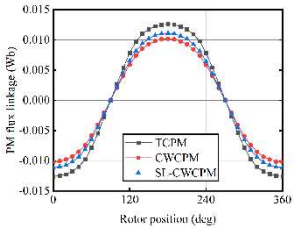

(a)

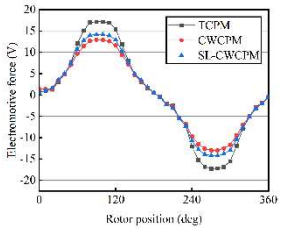

(b)

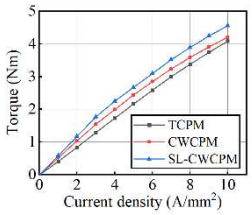

(c)

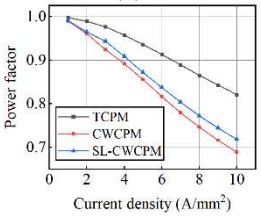

(d)

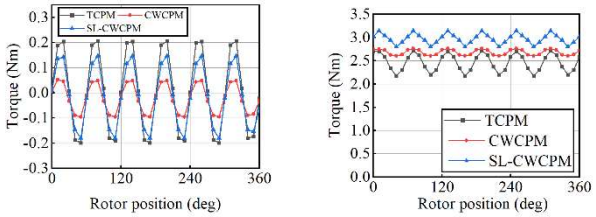

Fig.9. Performance comparison of three motors (a) PM flux linkage (b) no-load EMF (c) average torque versus the current density, (d) power factor versus the current density (e) cogging torque (f) torque waveform when current density equals 6 A/mm^2

Fig.10 shows the core loss and efficiency map of TCPM and SL-CWCPM. It can be seen that these two machines are with similar core loss and efficiency characteristic. It can be seen that SL-CWCPM has lower iron loss at low speeds, with a loss of 6W under 1500r/min, 6A/mm2 operating conditions, while TWCPM has a loss of 6.5W under the same operating conditions. At 3000r/min, the iron loss did not significantly increase with the increase of current density. When the speed is greater than 3000r/min, the iron loss significantly increases with the increase of current. And at high speeds and high currents, the iron loss of SL-CWCPM is greater than that of TCP. From an efficiency perspective, the efficiency of SL-CWCPM is significantly improved at low speed and current density. The efficiency of CWCPM is 0.935 at 1500r/min and 6A/mm2, while the efficiency of TCPM is 0.930, with an efficiency increase of 0.54%. The efficiency of SL-RCPM is significantly improved at low speed and current density.

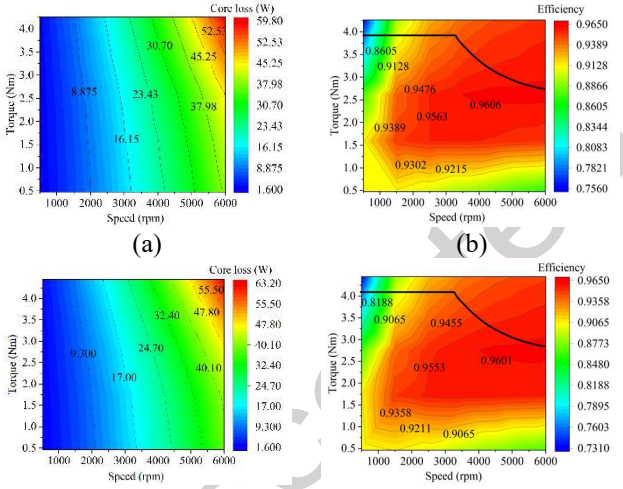

Fig.10. Loss and efficiency map (a) TCPM loss (b) TCPM efficiency (c)SL-CWCPM loss (d) SL-CWCPM efficiency

IV. HYBRID CORE CWCPM

A. Small size hybrid core CWCPM

The stator claw pole of CWCPM can be obtained by using the powder metallurgy technology as the SMC material is employed, then any complex core can be made. However, compared with silicon sheets, the permeability of SMC material is relative lower and the low frequency core loss is higher, thus the SMC is not a very good soft magnetic materials for manufacturing electrical machines in most cases. Silicon sheet is with high permeability, high flux saturation and it is a general soft magnetic material for fabricating electrical machines. Amorphous alloy material (AMM) is with very high permeability, very low core loss but lower flux saturation, it is now start to be employed in designing high frequency high efficiency electrical machines.

As the silicon sheets and AMM are usually made in lamination way to form the stator core or rotor core of electrical machine, and the fluxes are fluctuated in the lamination plane, it is very difficult to manufacture the stator claw pole by using these two materials. However, for the TCPM and CWCPM, these two materials can be used to make the stator yoke, and the stator claw pole wall and teeth are still made by using SMC. Through this kind of design, the performance of CWCPM can be improved further. The magnetic characteristic of SMC, silicon sheets and AMM are shown in Fig.11.

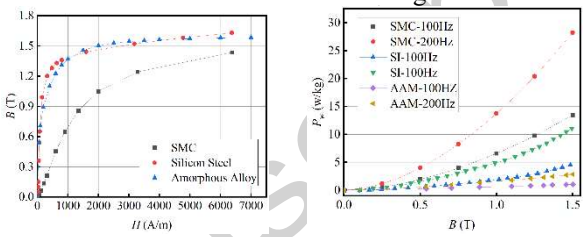

Fig.11. Permeability and loss characteristics of three materials. (a) Permeability characteristics (b) loss characteristics.

By using the 3D FEM, the main magnetic performance of CWCPM made all by SMC, hybrid silicon sheets and SMC, hybrid AMM and SMC are calculated respectively. Fig.12 shows the comparison of back EMF, PM flux linkage, average torque and power factor versus the input current density.

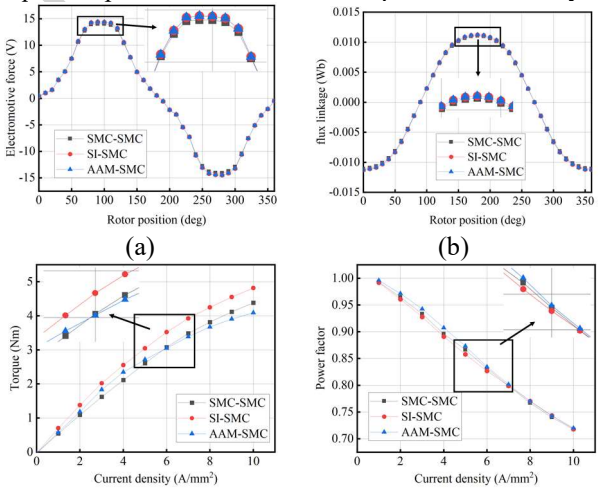

Fig.12. Performance comparison of three hybrid material cores CWCPM. (a) back EMF, (b) magnetic flux linkage (c) average torque versus the input current density (d) power factor versus the input current density.

Fig. 12(a) and (b) shows the no load back EMF and PM flux linkage of the three CWCPM with different stator core design. As shown, the no load back EMF and PM flux linkage of these machines are quite similar. Fig. 12(c) shows the torque comparison, it can be seen that by using the silicon sheets in the stator yoke, the torque performance has been increased greatly compared with the other machines. By using the AMM in the stator yoke, the CWCPM will have better performance than that of CWCPM made all by SMC cores when the input current density is lower than 6 A/mm2, however with the input current density increases the torque of CWCPM will be lower than that

all made by using SMC cores. The main reason is that though the AMM has higher permeability than that of SMC, it has much lower flux saturation than that of SMC. Fig. 12(d) shows the power factor of CWCPM made by using different materials. As shown, the power factor these machines decreases quickly with the input current density increases, and when the input current density is lower than 6 A/mm2, the power factor of CWCPM made by the hybrid silicon sheets and SMC is higher than the other two machines. For the core loss comparison, the calculated the core loss of CWCPM made by SMC, hybrid silicon sheets and SMC, hybrid AMM and SMC are 6W, 5.3 W, and 4.7 W, respectively when the rotor speed is 1500 r/min and the input current density is 6 A/mm2, as the core loss characteristic of silicon sheets and AMM are lower than that of SMC.

V. Prototype Manufacturing and Experimental Verification

To verify the concept of designing TCPM by using hybrid cores, a prototype machine is manufactured. Specifically, TCPM with hybrid silicon sheets and SMC was fabricated, considering the limitation of experimental conditions, its outer radius is 50 mm. Fig.13(a) and (b) show the key parts of the prototype, which including, stator claw pole, winding and stator yoke made by using silicon steel sheets. Fig.13(c) and (d) show the single-phase stator assembly diagram and the complete motor assembly diagram.

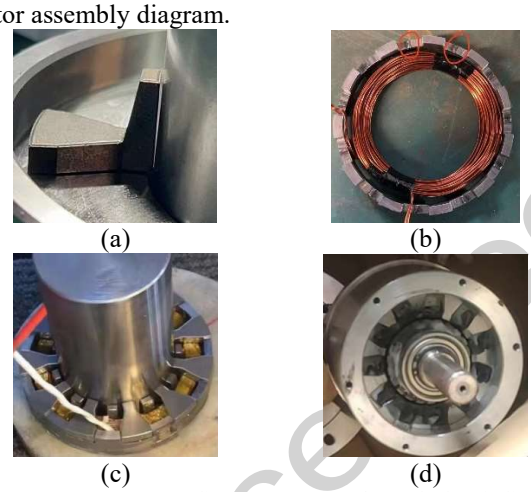

Fig.13. Prototype structure diagram. (a) stator claw pole (b) windings and stator yoke silicon steel laminations (c) the single-phase stator assembly diagram (d) complete motor assembly diagram

The performance of the prototype was tested by using the experimental platform shown in Fig.14. The experimental platform includes a dynamometer system, the signal acquisition system, a torque sensor, an oscilloscope and a liftable prototype stand. The dynamometer system can output constant speed (0-6000 r/min), the torque sensor has a range of 0-50 N·m and an accuracy of 0.1 N·m., and the four-channel oscilloscope can display three-phase waveforms simultaneously. The signal acquisition system (windows 10 system with java) can collect the data output from the speed sensor, torque sensor and oscilloscope for analysis and processing.

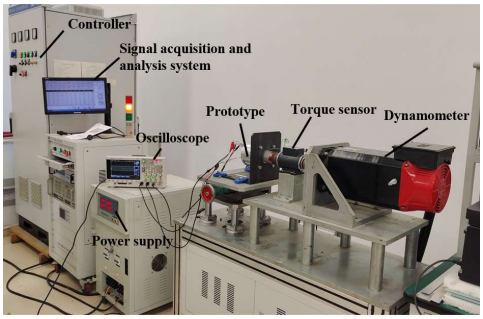

Fig.14. Experimental test platform

The torque transducer is JN-DN type, the dynamometer and its control system is made by AHD-01 type, the power supply is made by A-53 type, and the prototype is made by Wuxi Kelin Electric Motor Manufacturing Company after we provide the drawings to them.

Fig.15 shows the comparison of the tested and calculated no load back EMF of the prototype under the rotor speed of 200 r/min. As shown, back EMF of the prototype differ from each other by 120 degrees in phase, and the calculated no load back EMF of the machine is about 1.53V, and the magnitude of the measured back EMF is about 1.5V, which may be caused by the increase of the air gap length of the main magnetic circuit and the decrease of the magnetic conductivity due to the small air gap between the stator claw pole and the stator yoke during the manufacturing process. Based on the calculated and measured no load back EMF comparison, the basic concept of the TCPM made by using hybrid silicon sheets and SMC cores is verified.The experimental measurement of the no-load reverse electromotive force was 1.53 V, the 3rd harmonic amplitude was 0.05 V, and the harmonic distortion rate was 4.1%.

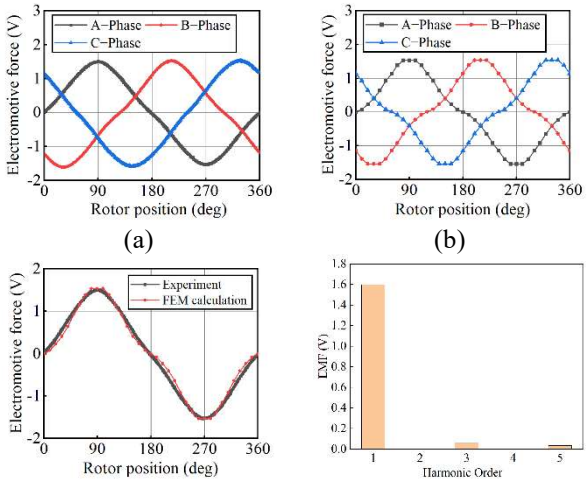

Fig.15. Comparison of experimental and test results, (a) measured three-phase EMF, (b) calculated three-phase EMF, (c) comparison of calculated and tested of A-phase EMF (d) Fourier decomposition analysis of A-phase EMF

The finite element simulation results and experimental measurements of the cogging torque are shown in Fig.16. From the figure, it can be seen that the peak value of the cogging torque obtained from the simulation is 0.81 N·m, and the peak value of the cogging torque measured experimentally is 0.85 N·m, and the experimental measurements are slightly larger than the simulation calculations, with an error of 4.94%.

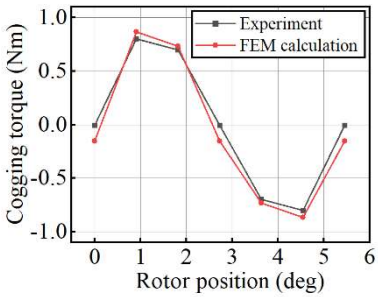

Fig.16. Finite element simulation value and experimental values of cogging torque

The motor load torque was measured at different current densities as shown in Fig.17. As the current density increases the error between the experimentally measured values and the finite element simulation values increases, at a current density of 3 A/mm2 the finite element simulation result is 1.2 N·m and the experimentally measured motor torque is 1.15 N·m with an error of 4.3%. At a current density of 9 A/mm2, the finite element simulation result is 3.2 N·m, and the experimentally measured torque of the motor is 3.05 N·m, with an error of 4.9%. The large error between the finite element simulation results of the average torque and the experimental measurements may be due to the presence of a spliced small air gap at the splices of the stator yoke module and the stator claw pole module, which results in a low experimental measurement of the average torque of the prototype.

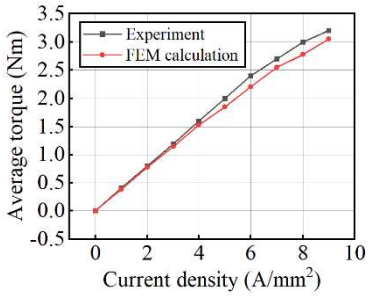

Fig.17. Finite element simulation value and experimental value of average torque under different current densities

VI. Conclusion

Combined the new concentrated winding and arranging the three-phase stator core in the circumferential way, a new CWCPM is developed, compared with the traditional TCPM, the proposed CWCPM can be applied in design references with shorter circumferential lengths. The CWCPM proposed in this paper can obtain higher average torque at the same current density, lower iron consumption and higher efficiency at rated operating conditions compared to TCPM. The design method of adding auxiliary poles can make up the cogging space between three-phase stators arranged in the same circumference and reduce the cogging torque and torque pulsation of the motor. Finally the prototype of TCPM with hybrid silicon sheets and SMC cores re manufactured to verify the analysis method employed in this paper.

References

[1] Tong W, Li S, Pan X, et al. Analytical Model for Cogging Torque Calculation in Surface-Mounted Permanent Magnet Motors with Rotor Eccentricity and Magnet Defects[J].IEEE Transactions on Energy Conversion, 2020, 35(4): 2191 - 2200.

[2] Tong W , Dai S , Li S ,et al.Modeling and Analysis of Axial Flux Permanent Magnet Machines With Coexistence of Rotor Radial Deviation and Angular Eccentricity[J].IEEE Transactions on Energy Conversion, 2020, 35(4): 2181 - 2190.

[3] Nasiri-Zarandi R , Ajamloo A M , Abbasazdeh K .Design Optimization of a Transverse Flux Halbach-Array PM Generator for Direct Drive Wind Turbines[J].IEEE Transactions on Energy Conversion, 2020, 35(3): 1485 - 1493.

[4] Zhang W , Xu Y , Zhou G .Research on a Novel Transverse Flux Permanent Magnet Motor With Hybrid Stator Core and Disk-Type Rotor for Industrial Robot Applications[J].IEEE Transactions on Industrial Electronics, 2021, 68(11): 11223-11233.

[5] Xu W , Li X , Zhu J ,et al.3D Modelling and Testing of a Stator-Magnet Transverse-Flux Linear Oscillatory Machine for Direct Compressor Drive[J].IEEE Transactions on Industrial Electronics, 2020, PP(99):1-1.

[6] Yang X , Kou B , Luo J ,et al.A Novel Dual-Consequent-Pole Transverse Flux Motor and Its Analytical Modeling[J].IEEE Transactions on Industrial Electronics, 2020, 37(2):1253-1278.

[7] Murali V , Joseph C C , Ravichandran M H ,et al.A Comprehensive Study on Transverse Flux Motor for Direct Drive Low-Speed Spacecraft Applications[J].IEEE Transactions on Industrial Electronics, 2021, 68(1):1120-1135

[8] Liu C, Zhu J, Wang Y, et al. Design considerations of PM transverse flux machines with soft magnetic composite cores[J]. IEEE Transactions on Applied Superconductivity, 2016, 26(4): 1-5.

[9] Zhang W , Xu Y , Sun M .Design of a Novel Claw Pole Transverse Flux Permanent Magnet Motor Based on Hybrid Stator Core[J].IEEE Transactions on Magnetics, 202157(6):11253-11265.

[10] Liu C, Chao Z, Wang S, et al. A quick electromagnetic performance analysis method for permanent magnet claw pole machine based on combined analytical and equivalent magnetic circuit method[J]. Electrical Engineering, 2023, 105(3): 1541-1553.

[11] Liu C , Wang D, Wang S, et al. A novel flux reversal claw pole machine with soft magnetic composite cores[J]. IEEE Transactions on Applied Superconductivity, 2020, 30(4): 1-5.

[12] W. Zhang, Y. Xu and M. Sun. Design of a Novel Claw Pole Transverse Flux Permanent Magnet Machine Based on Hybrid Stator Core[J]. IEEE Transactions on Magnetics, 2021, 57(6): 1-5.

[13] Y. Li, Z. Yu, H. Meng, J. Wang, et al. Design and Optimization of Hybrid-Excited Claw-Pole Machine for Vehicle[J]. IEEE Transactions on Applied Superconductivity, 2021, 31(8): 1-4

[14] Chu S, Liang D, Jia S, et al. Research and analysis on design characteristics of high-speed permanent magnet claw pole motor with soft magnetic composite cores for wide temperature range[J]. IEEE Transactions on Industry Applications, 2022, 58(6): 7201-7213.

[15] Leitner S, Saed N, Muetze A. Analysis of claw deflections and radial magnetic forces in low-cost sub-fractional horsepower BLDC claw-pole motors[C]. 2021 IEEE Energy Conversion Congress and Exposition (ECCE). 2021: 1-6.

[16] C. Liu, X. Li, G. Lei ,et al. Performance Evaluation of an Axial Flux Claw Pole Machine With Soft Magnetic Composite Cores[J]. IEEE Transactions on Applied Superconductivity, 2018, 28(4):1-5.

[17] C. Liu, D. Wang, S. Wang,et al. Design and Analysis of a New Permanent Magnet Claw Pole Machine With S-Shape Winding[J].IEEE Transactions on Magnetics, 2020, 37(3):1556-1569.

[18] Chen Y, Cai T, Zhu X, et al. Optimization of a new asymmetric-hybrid-PM machine with high torque density and low torque ripple considering the difference of magnetic materials[J]. IEEE Transactions on Magnetics, 2022, 58(2):1-5.

[19] Ibrahim I, Silva R, Mohammadi M H, et al. Surrogate models for design and optimization of inverter-fed synchronous motor drives[J]. IEEE Transactions on Magnetics, 2021, 57(6): 1-5

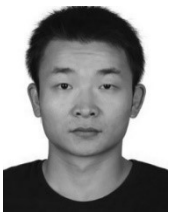

Chengcheng Liu (S'14-M'17) was born in Jiangsu, China,in 1988. He received the B.E. degree in automation from Yangzhou University, Yangzhou, China,in 2010. He is currently working toward the Ph.D.degree in electrical engineering at the Hebei University of Technology, Tianjin, China. He is also a joint Ph.D. student funded by the China Scholarship Council with the University of Technology, Sydney, NSW,Australia.

His research interests include the design, analysis, and control of permanent magnet machines.

Hongming Zhang was born in Hebei, China,in 1998. He received the B.E. degree in automation from Hebei University of Technology, Tianjin China,in 2021. He is currently working toward the master's degree in electrical engineering at the Hebei University of Technology, Tianjin, China.

His research interests include the Motor design optimization method and strategy.

Dianli Lv received the M.Eng. and Ph.D. degrees from Hebei University of Technology, Tianjin, China, in 2005 and 2011, respectively. His Ph.D. research was on numerical calculation and optimization of electromagnetic field, which was supported by Youhua Wang. Since 2005, he has been a member of the Electrical School, Hebei University of Technology. From April 2014 to April 2020, he did a postdoctoral project with the Department of Mechanical Engineering, Hebei University of Technology. He is with the State Key Laboratory of Reliability and Intelligence of Electrical Equipment and the Key Laboratory of Electromagnetic Field and Electrical Apparatus Reliability of Hebei Province, Hebei University of Technology. He has engineering experience in electric field analysis of transformer main insulation.

Feng Niu (M'15) was born in Hebei, China, in 1986. He received the B.S. and Ph.D. degrees from Hebei University of Technology, Tianjin, China, in 2009 and 2015, respectively, both in electrical engineering.,He is currently a Postdoctoral Research Fellow with the College of Electrical Engineering, Zhejiang University, Hangzhou, China. From September 2012 to September 2014, he was a Research Fellow with the Electrical Machines and Drives Laboratory, Michigan State University, East Lansing, MI, USA. He has coauthored more than 30 technical articles. His research interests include motor system and control, power converter control, and intelligent electrical equipment.

Gang Lei (M'14-SM'22) received the B.S. degree in Mathematics from Huanggang Normal University, China, in 2003, the M.S. degree in Mathematics and Ph.D. degree in Electrical Engineering from Huazhong University of Science and Technology, China, in 2006 and 2009, respectively.

He is currently a Senior Lecturer at the School of Electrical and Data Engineering, University of Technology Sydney (UTS), Australia. His research interests include computational electromagnetics, design optimization and control of electrical drive systems and renewable energy systems. He is an Associate Editor of the IEEE TRANSACTIONS ON INDUSTRIAL ELECTRONICS, and an Associate Editor of the TRANSACTIONS ON ENERGY CONVERSION.

Youhua Wang (M'14-SM'22) He received his B.S., M.S. and Ph.D. degrees in electrical engineering from Xi'an Jiaotong University, Hebei University of Technology and Fuzhou University in 1987, 1990 and 1994, respectively. His research interests include integrated effects of engineering electromagnetic fields.

Jianguo Zhu (S'93–M'96–SM'03) received the B.E. degree in 1982 from Jiangsu Institute of Technology, Jiangsu, China, the M.E. degree in 1987 from Shanghai University of Technology, Shanghai, China, and the Ph.D. degree in 1995 from the University of Technology Sydney (UTS), Sydney, Australia, all in electrical engineering.

He was appointed a lecturer at UTS in 1994 and promoted to full professor in 2004 and Distinguished Professor of Electrical Engineering in 2017. At UTS, he has held various leadership positions, including the Head of School for School of Electrical, Mechanical and Mechatronic Systems and Director for Centre of Electrical Machines and Power Electronics. In 2018, he joined the University of Sydney, Australia, as a full professor and Head of School for School of Electrical and Information Engineering. His research interests include computational electromagnetics, measurement and modelling of magnetic properties of materials, electrical machines and drives, power electronics, renewable energy systems and smart micro grids.